Int. J. Solids Structures, 1977, Vol. 13, pp. 1007–1017. Pergamon Press. Printed in Great Britain

INTERNAL FRACTURES IN SPHERES DUE TO STRESS WAVE FOCUSING

J. F. SILVA GOMES and S. T. S. AL-HASSANI

Department of Mechanical Engineering, The University of Manchester Institute of Science and Technology, Manchester M60 1QD, England

(*Received* 3 *January* 1977; *revised* 13 *May* 1977)

Abstract—The locations and times of occurrence of internal fractures in Perspex spheres subjected to localized explosive loading are investigated. An analysis of stress wave reflection from free boundaries based on the method of geometrical acoustics is found to give predictions which are in good agreement with results obtained from high speed photographs.

NOTATION

t time
$p(t)$ pressure function
$\mathbf{u}$ displacement vector
$\mathbf{v}$ particle velocity vector
V jump in particle velocity at the wave front
c_L dilatational wave speed
c_T distorsional wave speed
c_0 wave velocity of incident wave
c_1 wave velocity of reflected P-wave
c_2 wave velocity of reflected S-wave
E Young's modulus
x cartesian coordinates, in general
K subscript and superscript referring to the wave front
R_K, S_K principal radii of curvature of the wave front
R_S, S_S principal radii of curvature of the boundary
ϕ scalar potential for irrotational strain
ψ vector potential for distorsional strain
λ Lame's constant
μ Lame's constant
ν Poisson's ratio
ρ density
$\tau(x)$ wave function
ξ unit vector normal to the wave front
$\zeta^{(1)}$ unit vector normal to the boundary
$\zeta^{(2)}, \zeta^{(3)}$ unit vectors tangent to the boundary
σ_{ij} stress tensor
θ_0 angle of incidence
θ_1 angle of reflection of the P-wave
θ_2 angle of reflection of the S-wave
Γ boundary surface
∇ gradient operator $\left[=\left(\frac{\partial}{\partial x_1}, \frac{\partial}{\partial x_2}, \frac{\partial}{\partial x_3}\right)\right]$
∇^2 Laplacian operator $\left(=\frac{\partial^2}{\partial x_1^2}+\frac{\partial^2}{\partial x_2^2}+\frac{\partial^2}{\partial x_3^2}\right)$.

INTRODUCTION

The propagation of stress discontinuities in an elastic medium has been the subject of a number of investigations for sometime, and an early contribution in this field is that due to Friedlander[1]. The relevant theoretical concepts of the topic are also outlined by Keller[2], and some applications of the ray theory and wave front analysis to the problem of stress wave propagation through cylindrical and spherical inclusions embedded in an elastic medium can be found in [3–7]. A comprehensive analysis on the propagation of a plane shock wave front through a lens-shaped elastic body has recently been reported by Ting and Herrmann[8]. Their predictions of the displacement at the rear surface of the body were in very good agreement with the experimental results. At much the same time, Lovell *et al.*[9] have studied the internal fracturing behaviour of a Perspex sphere subjected to localised explosive shock loading at one

pole. Three fairly concentrated regions of fracture were identified in the vicinity of the anti-pole. Subsequently, high speed photographs of the development of the fractures were taken by Silva Gomes *et al.*[10], and the times of their occurrence were determined.

The authors feel that theoretical work on the development of internal fractures due to stress wave focusing in solids has been rather meagre. It is, however, hoped that the present investigation would shed some light on how the methods of wave front analysis may be easily employed to correctly predict the positions and extent of these fractures and even predict the order in time of their initiation.

ANALYSIS

The situation envisaged is that of a freely supported sphere subjected to a localised explosive pressure $p(t)$ at one pole P_0, Fig. 1. It is assumed that this pressure rises instantaneously to a certain value p and sharply decays to zero. Consequently, a stress

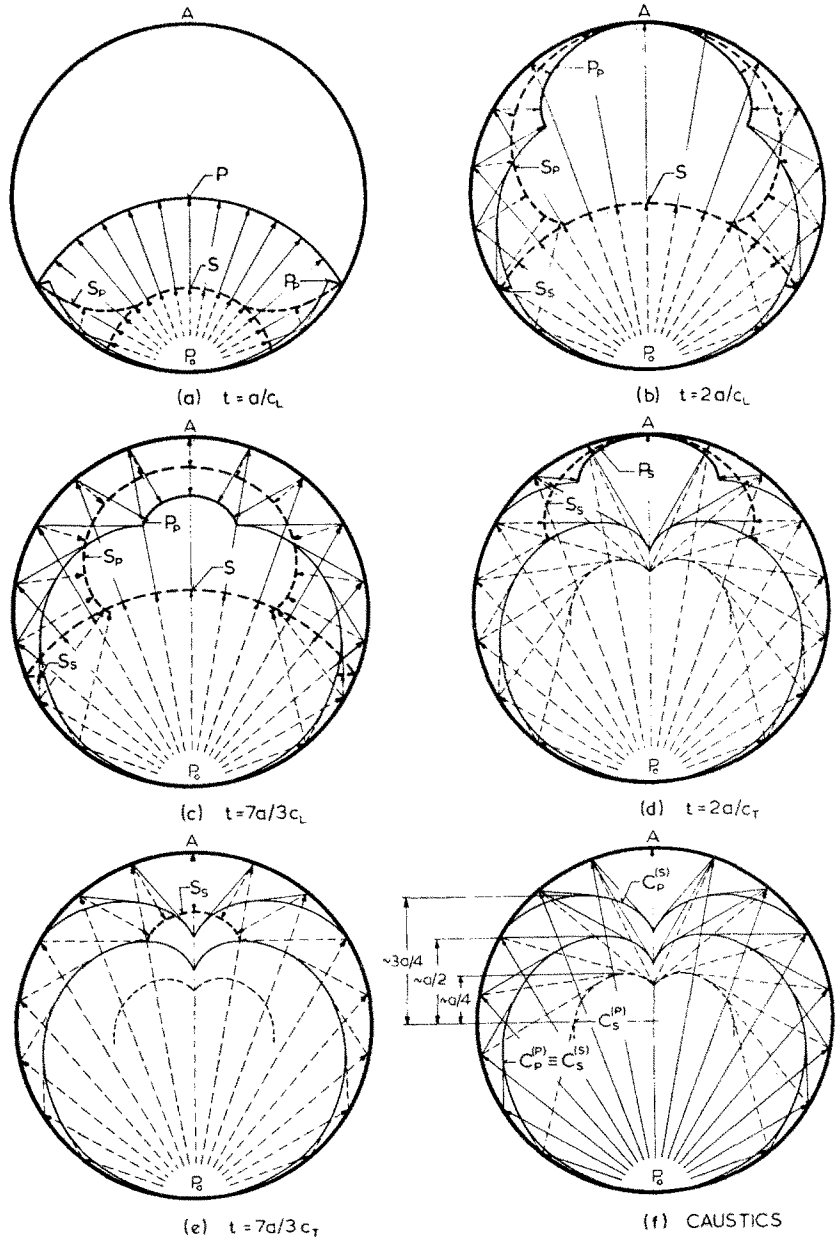

Fig. 1. Wave fronts in a sphere of Perspex material ($\nu = 0.35$) due to a point explosive loading at one pole. P_p, $C_p^{(p)}$—reflected P-wave front and caustic deriving from an incident P-wave. S_p, $C_s^{(p)}$—reflected S-wave front and caustic deriving from an incident P-wave. P_s, $C_p^{(s)}$—reflected P-wave front and caustic deriving from an incident S-wave. S_s, $C_s^{(s)}$—reflected S-wave front and caustic deriving from an incident S-wave.

discontinuity is engendered at the boundary which causes surfaces of discontinuity (wave fronts) to propagate into the interior of the sphere.

In Appendix A, it is shown that those surfaces of discontinuity travel with constant speeds, and that the jump in the particle velocity across the wave front at any time is related to its value at the initial wave front by the equation,

$$V = V_0\left[\frac{R_0 S_0}{RS}\right]^{1/2} \tag{1}$$

where R_0 and S_0 are the principal radii of curvature of the initial wave front, and R and S are the instantaneous radii of principal curvature of the actual wave front at some position along the same ray.

In a two dimensional problem, where one of the principal radii of curvature, say S, is infinite, eqn (1) becomes,

$$V = V_0\left[\frac{R_0}{R}\right]^{1/2} \tag{2}$$

For a spherically symmetric wave front as in our case, $R = S$, we have,

$$V = V_0\frac{R_0}{R}. \tag{3}$$

Equation (1) governs the propagation of a signal along each ray so long as the medium remains elastic, homogeneous, isotropic and continuous. When the wave front encounters a free boundary it is reflected back into the body, resulting in wave fronts of differing magnitude angles and radii of curvature. The general theory describing the behaviour of the incident and reflected dilatational and shear wave fronts on and from the boundary is outlined in Appendix B. It is shown that on each ray a point may be reached within the body where one of the radii of principal curvature of a reflected wave front vanishes. Equation (1) would dictate that on such a point the particle velocity, and consequently the stress, becomes singular. The locii of these singular points are described by eqns (B30) and (B31) which, in general, define two distinct geometrical surfaces. When the incident wave front is spherical, and when the boundary is a surface of revolution, as in our case, the surface described by eqn (B31) then degenerates into a straight line coincident with the axis of the boundary. The surface described by eqn (B30), i.e. the locus of the centers of meridional curvature of the reflected wave front, is usually referred to as the *CAUSTIC*.

In the case of a homogeneous, isotropic elastic medium subjected to a "point" explosive loading on its surface, two spherical stress waves will emanate from the point of loading,† i.e. a dilatational wave (P-wave), and a slower moving shear wave (S-wave). On arrival at the boundary surface, they are reflected back into the interior of the body each giving rise, in general, to a P-wave and an S-wave. Some successive positions for each wave front at different times, and the development of caustics for a Perspex sphere ($\nu = 0.35$) are shown in Fig. 1. An initial P-wave incident at a point on the spherical boundary gives rise to a P-wave whose angle of reflection is the same as that of incidence (see eqn B12) and the corresponding wave front is denoted P_p; from the same incident P-wave, a reflected S-wave results in of smaller angle of reflection (see eqn B12), and the corresponding wave front is denoted S_p. Similarly, an S-wave incident at a point on the boundary gives rise to a reflected S-wave whose angle of reflection is the same as the angle of incidence, denoted S_s, and to a P-wave whose angle of reflection is larger and it is denoted P_s. (There are certain restrictions to this statement but we shall not pursue them here). The focus for P_p and S_s wave fronts are identical, and they constitute the fastest and slowest wave combination; the locus of all such focii is the caustic indicated by $C_p^{(p)}$ which is the same as $C_s^{(s)}$. The focii for P_s (i.e. $C_s^{(p)}$) and S_p (i.e. $C_p^{(s)}$) are different, as indicated in Fig. 1(f).

†Rayleigh surface waves are not considered in this paper.

If, in fact, the detonator gave an instantaneous rise to the pressure then a sharp fronted pulse would propagate, and the theory would predict that fracture should occur all along the caustic surface. However, in practice, the rise time of the pressure pulse is finite, and an infinite stress may not occur at the caustic. Instead, only a stress amplification would be produced which can cause fracture in the vicinity of the caustics and, in particular, at the uppermost regions and cusps. In fact, at the regions near the anti-pole, the angle of incidence is small and consequently the stresses associated with the reflected wave fronts are of higher intensity. Furthermore, in the vicinity of the cusps of the caustics, not only the meridional radius of curvature of a given reflected wave front vanishes, also its tangential radius becomes almost zero. Thus a second effect of stress amplification takes place. Therefore, if at all fractures have to take place, they are more likely to be expected between the uppermost regions and the cusps of the caustics. For high and very sharp pressure loading, the fractures may extend to other regions around the caustics to the extent of peeling out the upper surfaces of the sphere.

EXPERIMENTAL OBSERVATIONS

Spheres of 5.71 and 7.37 cm were machined from commercial grade Perspex acrylic stock. The material Properties of Perspex are[11], $E = 3.0 \times 10^9$ N/m^2, $\nu = 0.35$, and $\rho = 1.19 \times 10^3$ Kg/m^3, giving $c_L = 2011$ m/sec and $c_T = 966$ m/sec. The impulsive loading was secured by energizing I.C.I. electrical detonators bonded to the surface of the specimen, as indicated in Fig. 2.

For the purpose of observing the formation of fractures, the transparent sphere was placed between a camera and a flash tube, as illustrated in Fig. 2. The camera used was a Barr and Stroud ultra high speed type CP5 No. 69, the mirror of which can be accelerated to produce a maximum of 2,000,000 frames/sec. The explosive charge and the flash tube were automatically fired by the camera. Whenever a fracture appeared inside the specimen, the light would be diffracted through the region of fracture, and a differential intensity of exposure would be registered on the film.

Figure 3(a) shows a sequence of photographs taken at a rate of nearly 670,000 frames/sec (≈ 1.5 μsec between frames) for a 7.37 cm diameter Perspex sphere subjected to a localised explosive pressure on the periphery. Apart from the fracture beneath the area in direct contact with the explosive pressure, three other distinct regions of fracture, F-1, F-2, and F-3, can be observed. The high speed photographs show them to appear at different times in frames 2, 11 and 26, which are shown enlarged in Fig. 3(b). Frame 1 in the sequence corresponds to a time of

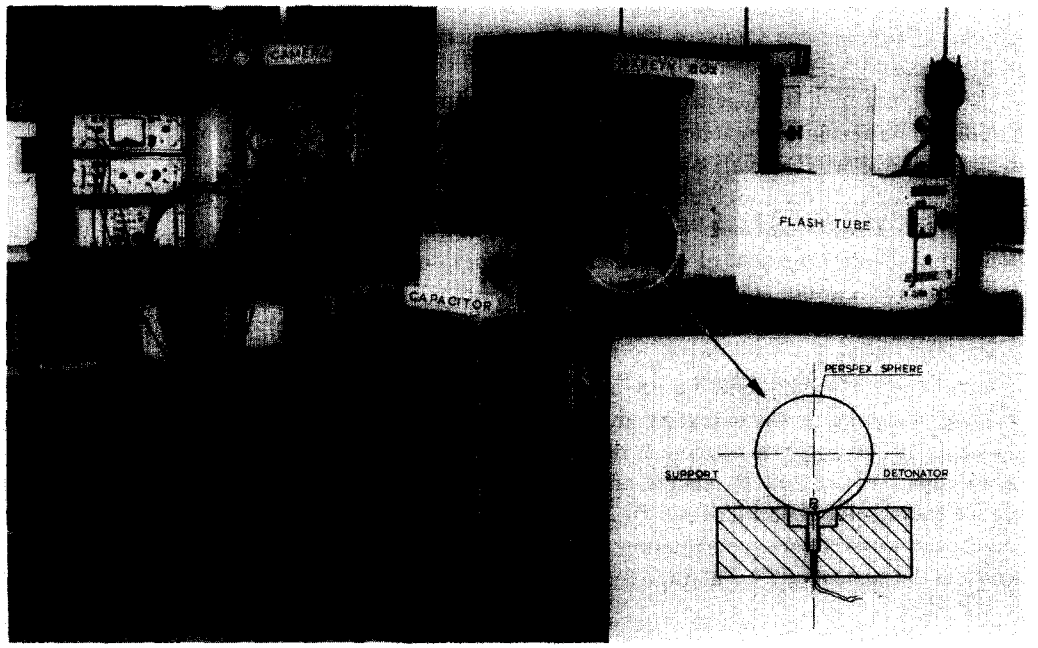

Fig. 2. Experimental set up, detonator positioning, and support arrangement.

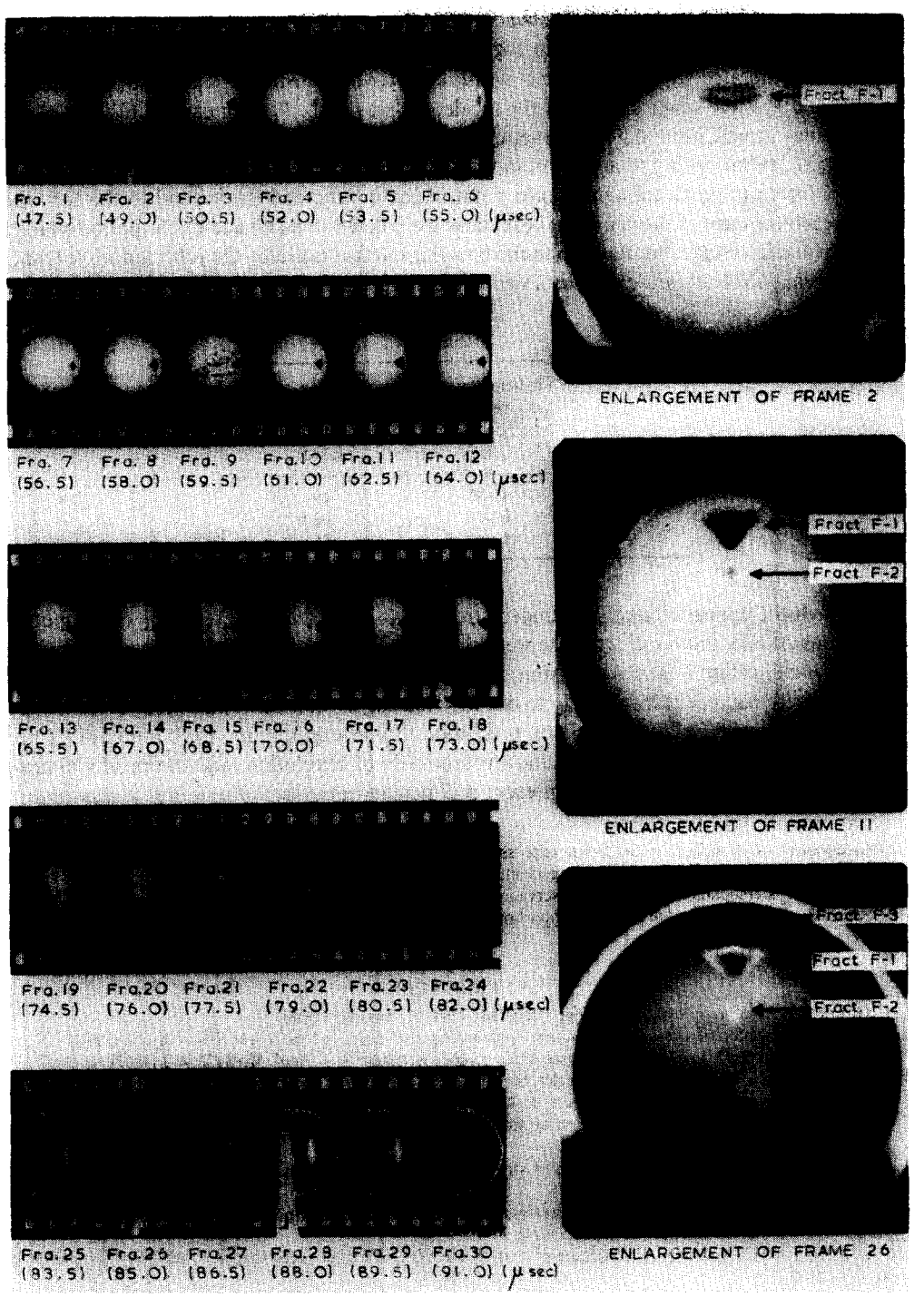

Fig. 3. Sequence showing the formation of internal fractures in a 7.37 cm diameter Perspex sphere due to a point explosive loading at one pole. (Framing speed, approx. 670,000 frames/sec).

47.5 μsec after detonation. The actual shape and position of the fractures were determined by stereophotomicrography and later by cutting each sphere into two halves and making direct observations on a meridional section of the specimen.

COMPARISONS AND DISCUSSION

The times at which the different fractures took place, as well as their position in relation to the point of loading, indicate that they are associated with the different types of stress waves that are generated inside the sphere. Fracture F-1 is thought to be initiated by the reflected P_p

wave but later reinforced by the reflected S_s wave and its position matches well with the upper region of the caustic $C_p^{(p)}$ and $C_s^{(s)}$ in Fig. 1(f). Fracture F-2 we associate with the reflected shear wave generated by the incident P-wave, i.e. S_p with caustic $C_s^{(p)}$, and fracture F-3 with the reflected P-wave originating from the incident S-wave, i.e. P_s with caustic $C_p^{(s)}$.

The times at which the different fractures would make their appearance are calculated, and two magnitudes for each one are given in the table below. The first refer to the time taken by the wave fronts to reach the upper-most point of the caustic and the second to the time they take to reach the cusp of the caustic. These times were determined by adding the period which an incident wave front takes to travel up to the boundary to that taken by the reflected wave front to reach the caustic. They are evidently in good agreement with what was found experimentally.

Table 1.

Fracture	Predicted time of occurrence after detonation (μsec)	Time observed experimentally (μsec)
F-1	43–50	49
F-2	62–67	62.5
F-3	80–86	85

Although the appearance of unbounded stresses, as given from the methods of geometrical optics, is physically unrealistic, the theoretical predictions may be useful in revealing an effect of stress amplification at the wave front, and hence giving some indication in identifying the locations where damage is more likely to occur. The analysis can easily be extended to solids of other shapes, in particular to solids of revolution. Some experiments have already[12] been performed on ellipsoids, paraboloids and hyperboloids of revolution, and the results obtained strongly reinforce the success of the present rudimentary analysis.

Acknowledgements—The authors would like to express their gratitude to Professor W. Johnson, University of Cambridge (U.K.), for his useful comments and encouragement, and to Dr. S. Turner, of I.C.I. (Plastics division) for his kind assistance in the stereophotomicrographic observations. They also acknowledge Instituto Nacional de Investigação Científica, Lisbon, Portugal, for the financial support of the first author.

REFERENCES

1. F. G. Friedlander, *Sound Pulses*. Cambridge University Press, Cambridge (1958).
2. H. Keller, Propagation of stress discontinuities in inhomogeneous elastic media. *SIAM Review* **6**, 356 (1964).
3. T. C. T. Ting and E. H. Lee, Wave front analysis in composite materials. *J. Appl. Mech.* **36**, 497 (1969).
4. J. D. Achenbach, J. H. Hemann and F. Ziegler, Separation at the interface of a circular inclusion and the surrounding medium under an incident compressive wave, *J. Appl. Mech.* **37**, 298 (1970).
5. T. C. T. Ting and S. C. Chou, Propagation of stress gradient through an inclusion—Part 1. *J. Appl. Mech.* **40**, 711 (1973).
6. T. C. T. Ting and S. C. Chou, Propagation of stress gradient through an inclusion—Part 2. *J. Appl. Mech.* **40**, 718 (1973).
7. J. H. Griffin and J. Miklowitz, Wave front analysis of a plane compressional pulse scattered by a cylindrical elastic inclusion. *Int. J. Solids Structures* **10**, 1333 (1974).
8. T. C. T. Ting and G. Herrmann, Propagation of a shock wave front through a lens-shaped elastic body. *J. Appl. Mech.* **41**, 691 (1974).
9. E. Lovell, S. T. S. Al-Hassani and W. Johnson, Fracture in solid spheres and circular disks due to a point explosive impulse on the periphery. *Int. J. Mech. Sci.* **16**, 193 (1974).
10. J. F. Silva Gomes, W. Johnson and S. T. S. Al-Hassani, A note on times to fracture in solid perspex spheres due to point explosive loading. *Int. J. Mech. Sci.* **18**, 543 (1976).
11. I.C.I., *The Properties of Perspex Acrylic Materials*. I.C.I. Publication, Plastics Division, Herts, England.
12. S. T. S. Al-Hassani and J. F. Silva Gomes, Fracturing of brittle solids of revolution due to stress wave focusing, (to be published).

APPENDIX A

The propagation of wave fronts in a homogeneous isotropic elastic solid

As mentioned in the Introduction, the general analytical treatment of wave front analysis and ray theory can be found in [1] and [2]. However, in order to clarify the most relevant topics involved in this type of analysis, we shall reproduce here, and in Appendix B, some of its fundamental concepts. These are presented in a simplified manner, orientated towards the particular situation corresponding to the problem analysed in the present paper.

Let $\mathbf{u}$ be the displacement vector which can be expressed in terms of a scalar potential ϕ and a vector potential ψ in the form,

$$\mathbf{u} = \nabla\phi + \nabla \times \psi \tag{A1}$$

where the potentials ϕ and ψ satisfy the equations,

$$\nabla^2\phi = \frac{1}{c_L^2}\frac{\partial^2\phi}{\partial t^2} \quad \text{with} \quad c_L^2 = \frac{\lambda + 2\mu}{\rho} \tag{A2}$$

and

$$\nabla^2\psi = \frac{1}{c_T^2}\frac{\partial^2\psi}{\partial t^2} \quad \text{with} \quad c_T^2 = \frac{\mu}{\rho} \tag{A3}$$

where λ and μ are the Lamé constants, and ρ is the density.

Since $c_L > c_T$, the scalar potential ϕ corresponding to a longitudinal stress pulse is governed by a wave equation with a greater wave velocity than the distorsional wave described by ψ. Hence, for a wave moving into an undisturbed medium, the region adjacent to the leading wave front corresponds to zero ψ, until the instant when the slower distorsional wave arrives. The former is referred to as the P-wave front and the latter as the S-wave front. If $\tau(x) = t$ gives the position at time t of either the P-wave front or the S-wave front, it has been established [1–6] that the wave function $\tau(x)$ must satisfy the eikonal equation,

$$\nabla\tau \cdot \nabla\tau = \frac{1}{c^2} \tag{A4}$$

where $c = c_L$ for a P-wave front, and $c = c_T$ for an S-wave front.

The orthogonal trajectories of the family of wave fronts given by equation $\tau(x) = t$ are the rays, and for a homogeneous, isotropic elastic medium they are straight lines. The unit vector normal to the wave front, i.e. parallel to the ray, is given by,

$$\xi(x) = \frac{1}{|\nabla\tau|}\nabla\tau$$

or, from eqn (A4),

$$\xi(x) = c\nabla\tau(x) \tag{A5}$$

It can also be shown (see Ref. [2], for example) that jumps in the stress and the particle velocity, $v_i = \partial u_i/\partial t$, are related by the equation,

$$[\sigma_{ij}]\xi_j = -\rho c[v_i] \tag{A6}$$

where c represents the wave speed, and the jumps in field quantities are indicated by the usual bracket notation. In the case of a P or a dilatational wave, the velocity jump is normal to the surface of discontinuity and for an S or shear wave, the velocity jump is tangential to the surface of discontinuity.

To consider the determination of the magnitude of the propagating discontinuity, we assume that the material is undisturbed before the wave front arrives. Thus, if the wave front is $\tau(x) = t$, the jump in $\mathbf{v}$ can be represented by,

$$\mathbf{V}(x) = [\mathbf{v}(x, t)]_{t=\tau(x)} = \mathbf{v}(x, \tau(x)) \tag{A7}$$

and, if V_0 represents the amplitude of the pulse at the initial wave front, it can be shown that the jump in particle velocity at the actual wave front is given by,

$$V = V_0\left[\frac{R_0 S_0}{RS}\right]^{1/2} \tag{A8}$$

where R_0 and S_0 are the principal radii of curvature of the initial wave front, and R and S are the principal radii of curvature of the actual wave front, at position $x = x(s)$ on the ray, s being the length of the arc measured along the ray.

APPENDIX B

The reflection of a spherical wave front from an axially symmetric boundary

Let the boundary Γ be represented by three equations of the form,

$$x = g(\alpha, \beta) \tag{B1}$$

and assume that the surface Γ and its parametrization are such that two distinct tangent vectors and a unit normal at each point are given by,

$$\eta^{(\alpha)} = g_\alpha, \quad \eta^{(\beta)} = g_\beta \quad \text{and} \quad \zeta^{(1)} = \frac{\eta^{(\alpha)} \times \eta^{(\beta)}}{|\eta^{(\alpha)} \times \eta^{(\beta)}|}$$

respectively. The positive direction of vector $\zeta^{(1)}$ is directed to the outside of Γ. The incident family of wave fronts can be specified as,

$$\tau^{(0)}(x) - t = 0 \tag{B2}$$

where

$$\nabla\tau^{(0)} \cdot \nabla\tau^{(0)} = \frac{1}{c_0^2} \tag{B3}$$

and the unit vector normal to the wave front, in the direction of propagation, is

$$\xi^{(0)} = c_0 \nabla\tau^{(0)} \tag{B4}$$

For an incident P-wave, we have

$$\xi^{(0)} \times \mathbf{V}^{(0)} = 0, \quad \text{with} \quad c_0 = c_L,$$

and for an incident S-wave,

$$\xi^{(0)} \cdot \mathbf{V}^{(0)} = 0, \quad \text{with} \quad c_0 = c_T,$$

where $\mathbf{V}^{(0)}$ represents the incident signal at the boundary.

When the incident wave front reaches the boundary, it can no longer be assumed that only the original P or S wave is present in the medium. It is well known that when a ray is incident upon a free boundary, it produces, in general, two reflected rays—one corresponding to a dilational wave, and the other to a shear or distorsional wave. If these two reflected wave fronts are represented by equations of the form,

$$\tau^{(K)}(x) = t, \quad \text{with} \quad K = 1, 2, \tag{B5}$$

the wave functions $\tau^{(K)}(x)$ and the unit normals $\xi^{(K)}$ are determined by,

$$\nabla\tau^{(K)} \cdot \nabla\tau^{(K)} = \frac{1}{c_K^2} \quad \text{and} \quad \xi^{(K)} = c_K \nabla\tau^{(K)}, \quad \text{with } K = 1, 2. \tag{B6}$$

If $\mathbf{V}^{(1)}$ and $\mathbf{V}^{(2)}$ represent the P and S reflected signals, respectively, we have,

$$\xi^{(1)} \times \mathbf{V}^{(1)} = 0 \quad \text{with} \quad c_1 = c_L \tag{B7}$$

and

$$\xi^{(2)} \cdot \mathbf{V}^{(2)} = 0 \quad \text{with} \quad c_2 = c_T \tag{B8}$$

As both reflected wave fronts emerge from the intersection of the incident wave front with the boundary Γ we can write, from eqn (B1),

$$\tau^{(K)}(g(\alpha, \beta)) = \tau^{(0)}(g(\alpha, \beta)), \quad \text{with } K = 1, 2. \tag{B9}$$

Also, since the wave fronts always are joined at surface Γ, and because their directional derivatives must be equal, then

$$\nabla\tau^{(K)} \cdot g_\alpha = \nabla\tau^{(0)} \cdot g_\alpha, \quad \text{and} \quad \nabla\tau^{(K)} \cdot g_\beta = \nabla\tau^{(0)} \cdot g_\beta$$

or,

$$[c_K \xi^{(0)} - c_0 \xi^{(K)}] \cdot \eta^{(\alpha)} = 0, \quad \text{and} \quad [c_K \xi^{(0)} - c_0 \xi^{(K)}] \cdot \eta^{(\beta)} = 0 \tag{B10}$$

which implies that the vector in brackets must be parallel to $\zeta^{(1)}$, and therefore there exists a scalar a_K such that

$$\xi^{(K)} = \frac{c_K}{c_0} \xi^{(0)} + a_K \zeta^{(1)}, \quad \text{with } K = 1, 2, \tag{B11}$$

i.e. all three wave normals $\xi^{(K)}$ (with $K = 0, 1, 2$) and the normal to the boundary, $\zeta^{(1)}$, are coplanar. The relative positions of these vectors are illustrated in Fig. 4. The unit vector $\zeta^{(2)}$, in the same plane, is tangent to Γ and its direction is defined by the angle $\theta_0 (0 \leq \theta_0 \leq \pi/2)$, such that $\xi^{(0)} \cdot \zeta^{(2)} = \sin\theta_0$. From Fig. 4 it can be deduced that,

$$\xi^{(K)} \cdot \zeta^{(1)} = \cos\theta_K, \quad \text{and} \quad \xi^{(K)} \cdot \zeta^{(2)} = \sin\theta_K$$

and, by taking the scalar product of each equation in (B11) with $\zeta^{(1)}$ and $\zeta^{(2)}$, it follows,

$$\frac{\sin\theta_K}{c_K} = \frac{\sin\theta_0}{c_0}, \quad \text{with} \quad K = 1, 2 \tag{B12}$$

and

$$a_K = \frac{\sin(\theta_0 - \theta_K)}{\sin\theta_0}, \quad \text{with } K = 1, 2. \tag{B13}$$

Also, from Fig. 4,

$$\xi^{(K)} = \cos\theta_K \zeta^{(1)} + \sin\theta_K \zeta^{(2)} \tag{B14}$$

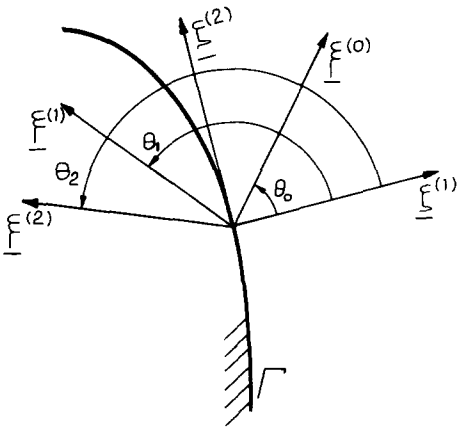

Fig. 4. Wave normals at the boundary.

and thus, from eqns (B7) and (B8), we get

$$\mathbf{V}^{(1)} = \alpha_1 \cos\theta_1 \boldsymbol{\zeta}^{(1)} + \alpha_1 \sin\theta_1 \boldsymbol{\zeta}^{(2)} \tag{B15}$$

and

$$\mathbf{V}^{(2)} = \alpha_2 \sin\theta_2 \boldsymbol{\zeta}^{(1)} - \alpha_2 \cos\theta_2 \boldsymbol{\zeta}^{(2)} + \beta \boldsymbol{\zeta}^{(3)} \tag{B16}$$

where $\boldsymbol{\zeta}^{(3)} = \boldsymbol{\zeta}^{(1)} \times \boldsymbol{\zeta}^{(2)}$ and $\alpha_1, \alpha_2, \beta$, are three parameters to be calculated from the boundary conditions. The incident signal $\mathbf{V}^{(0)}$ can also be resolved in the above manner,

$$\mathbf{V}^{(0)} = \alpha_0 \cos\theta_0 \boldsymbol{\zeta}^{(1)} + \alpha_0 \sin\theta_0 \boldsymbol{\zeta}^{(2)} \tag{B17}$$

or,

$$\mathbf{V}^{(0)} = \alpha_0 \sin\theta_0 \boldsymbol{\zeta}^{(1)} - \alpha_0 \cos\theta_0 \boldsymbol{\zeta}^{(2)} + \beta_0 \boldsymbol{\zeta}^{(3)} \tag{B18}$$

for an incident P-wave or an incident S-wave, respectively.

The coefficients α_1, α_2, and β in eqns (B15) and (B16) can be determined from the condition of zero stress at the free boundary, and they are found to be

(a) for an incident P-wave

$$\begin{aligned} \beta &= 0 \\ \alpha_1 &= -\alpha_0\left[\frac{c_1^2\cos^2 2\theta_2 + c_2^2 \sin 2\theta_2 \sin 2\theta_0}{c_1^2\cos^2 2\theta_2 - c_2^2 \sin 2\theta_2 \sin 2\theta_0}\right] \\ \alpha_2 &= \alpha_0\left[\frac{2c_1c_2\cos 2\theta_2 \sin 2\theta_0}{c_1^2\cos^2 2\theta_2 - c_2^2 \sin 2\theta_2 \sin 2\theta_0}\right] \end{aligned} \tag{B19}$$

(b) for an incident S-wave

$$\begin{aligned} \beta &= \beta_0 \\ \alpha_1 &= -\alpha_0\left[\frac{2c_1c_2\cos 2\theta_0 \sin 2\theta_0}{c_1^2\cos^2 2\theta_0 - c_2^2 \sin 2\theta_1 \sin 2\theta_0}\right] \\ \alpha_2 &= -\alpha_0\left[\frac{c_1^2\cos^2 2\theta_0 + c_2^2 \sin 2\theta_1 \sin 2\theta_0}{c_1^2\cos^2 2\theta_0 - c_2^2 \sin 2\theta_1 \sin 2\theta_0}\right]. \end{aligned} \tag{B20}$$

At this stage we are able thus to calculate the reflected signals at points on the boundary surface. The ratio of the amplitudes of the reflected signals to the amplitude of the incident signal depends on the angle of incidence, and in Fig. 5 curves are plotted for a material such as Perspex, which has a Poisson's ratio of 0.35. For this material, it is found that the $V^{(1)}/V^{(0)}$ curve for an incident shear wave terminates at an angle 26.68° above which no dilatational wave is reflected.

To investigate the response of the reflected signals along each ray, we need to calculate the radii of principal curvature of the reflected wave fronts. Referring to Fig. 6, let R_S and R_0 be the radii of curvature on B of the boundary and of the incident wave front, respectively. At the same point B, represent by R_K ($K = 1, 2$) the radii of curvature of the reflected wave fronts. Considering a neighboring point B' on Γ, the angle of reflection at this point is

$$(\theta_K)_{B'} \approx \theta_K + \frac{d\theta_K}{d\theta_0}(\Delta\theta_0 - \Delta\theta) \tag{B21}$$

and

$$\Delta\theta_0 = \frac{BN}{R_0}, \quad \Delta\theta = \frac{BB'}{R_S}, \tag{B22}$$

$$\frac{d\theta_K}{d\theta_0}(\Delta\theta_0 - \Delta\theta) + \Delta\theta = \frac{B'M}{R_K} \tag{B23}$$

$$BN = BB'\cos\theta_0 \quad \text{and} \quad B'M = -BB'\cos\theta_K \tag{B24}$$

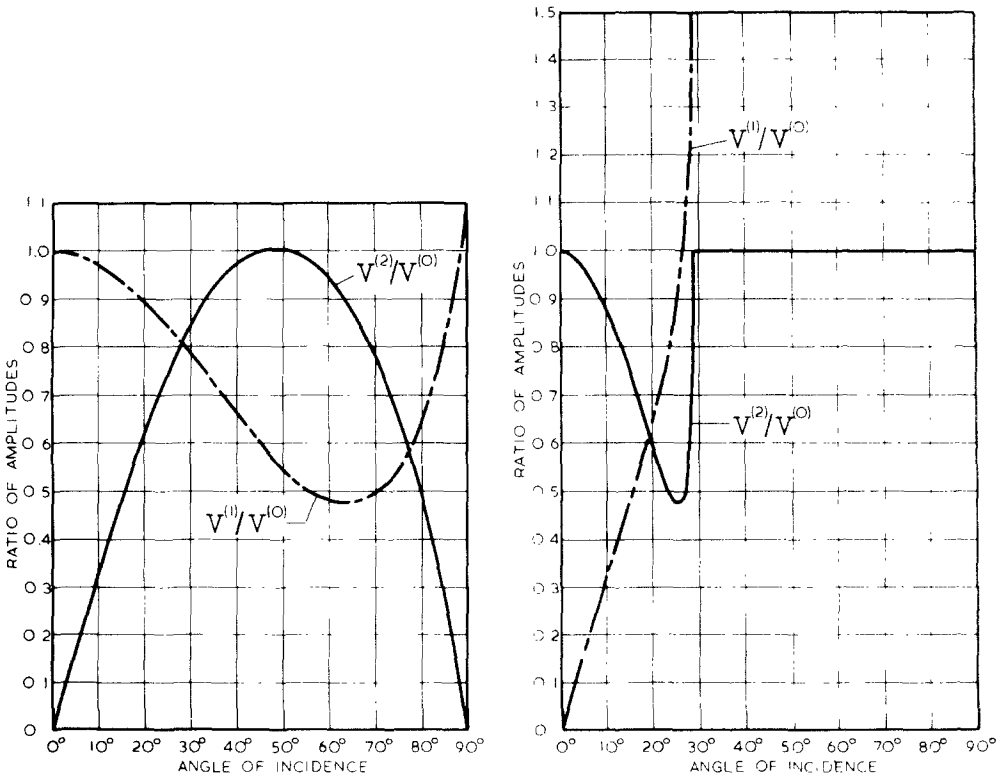

Fig. 5. Amplitudes of reflected dilatational and distortional waves at different angles of incidence, for $\nu = 0.35$. (a) Incident P-wave. (b) Incident S-wave.

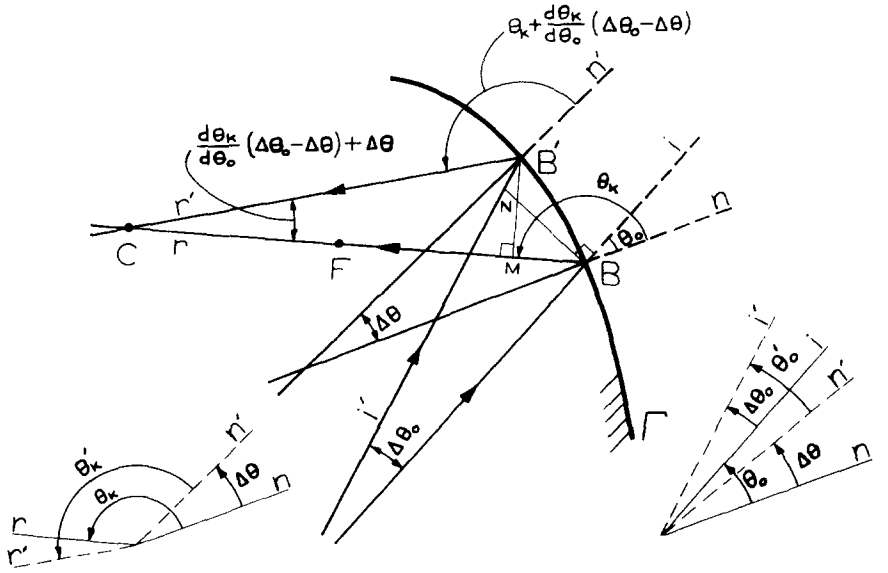

Fig. 6. Reflection geometry of two neighbouring rays.

Also, from eqn (B12), it follows that

$$\frac{d\theta_K}{d\theta_0} = \frac{\tan\theta_K}{\tan\theta_0} \tag{B25}$$

and combination of eqns (B21)–(B25) leads to,

$$R_K = -\left[\frac{\tan\theta_K}{\tan\theta_0}\left(\frac{\cos\theta_0}{R_0} - \frac{1}{R_S}\right) + \frac{1}{R_S}\right]^{-1} \cos\theta_K. \tag{B26}$$

Equation (B26) gives the position of the centre of curvature of the reflected wave front at point B on the boundary. This centre

lies on the corresponding ray at algebraic distance R_K measured from B towards the direction of propagation of the reflected wave. At any point F on the reflected ray, the radius of curvature is given by,

$$R_F = R_K - BF \tag{B27}$$

The problem under analysis is one of a class in which a spherical incident wave front is reflected at a surface of revolution and whose centre is on the axis of symmetry. In this case, the reflected wave fronts are also surfaces of revolution about the same axis, and the quantity given by equation (B26) is its meridional radius of curvature. The centre of tangential curvature lies on the axis of revolution, and a simple geometric analysis yields, see Fig. 7,

$$S_K = -S_S\left[\cos\theta_K - \sin\theta_K \frac{S_0\cos(\theta_K - \theta_0) - S_S\cos\theta_K}{S_0\sin(\theta_K - \theta_0) - S_S\sin\theta_K}\right]. \tag{B28}$$

Along the reflected ray, at point F, the tangential radius of curvature is given by,

$$S_F = S_K - BF \tag{B29}$$

and the jump in particle velocity at point F can now be calculated by using eqn (A8).

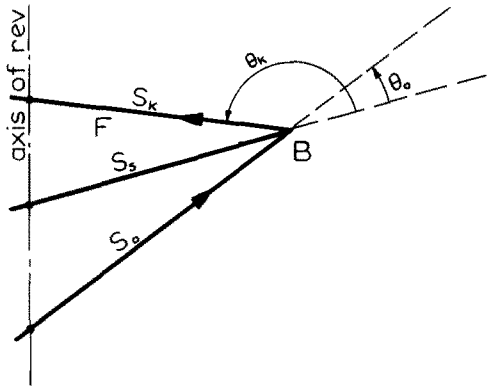

Fig. 7. Tangential radii of curvature.

From eqns (B27) and (B29) it transpires that on each ray, a point C may be reached where one of the radii of principal curvature of the reflected wave front vanishes, i.e.

$$BC = R_K \tag{B30}$$

or

$$BC = S_K. \tag{B31}$$

The locus of points C as given by eqn (B30) is the caustic. For an axisymmetric solid and for a spherical incident wave front centered on the axis of symmetry, the caustic is a surface of revolution about the same axis. The meridional section of the caustic can be easily obtained by use of eqns (B12) and (B26). Equation (B12) gives the direction of the reflected ray at each point on the boundary, and eqn (B26) determines the distance from the caustic to the boundary measured along the ray.